Temperature-Dependent Relaxation of Excitons in Tubular Molecular Aggregates: Fluorescence Decay and Stokes Shift

A. Pugžlys, R. Augulis, and P. H. M. van Loosdrecht

Materials Science Centre, University of Groningen, Nijenborgh 4, 9747 AG Groningen, The Netherlands

C. Didraga, V. A. Malyshev,† and J. Knoester*

Institute for Theoretical Physics and Materials Science Centre, University of Groningen, Nijenborgh 4, 9747 AG Groningen, The Netherlands

Received: May 16, 2006; In Final Form: July 21, 2006

We report temperature-dependent steady-state and time-resolved fluorescence studies to probe the exciton dynamics in double-wall tubular J-aggregates formed by self-assembly of the dye 3,3′-bis(3-sulfopropyl)-5,5′,6,6′-tetrachloro-1,1′-dioctylbenzimidacarbocyanine. We focus on the lowest energy fluorescence band, originating from the inner cylindrical wall. At low temperatures, the experiments reveal a nonexponential decay of the fluorescence, with a typical time scale that depends on the emission wavelength. At these temperatures we also find a dynamic Stokes shift of the fluorescence spectrum and its nonmonotonic dependence on temperature under steady-state conditions. All these data indicate that below about 20 K the excitons in the lowest fluorescence band do not reach thermal equilibrium before emission occurs, while above about 60 K thermalization on this time scale is complete. By comparing the two lowest fluorescence bands, we also find indications for fast energy transfer from the outer to the inner wall. We show that the Frenkel exciton model with diagonal disorder, which previously has been proposed to explain the absorption and linear dichroism spectra of these aggregates, yields a quantitative explanation to the observed dynamics. To this end, we extend the model to account for weak phonon-induced scattering of the localized exciton states; the spectral dynamics are then described by solving a Pauli master equation for the exciton populations.

I. Introduction

The optical properties and the dynamics of Frenkel excitons in self-assembled aggregates of organic molecules has had a long history already.[1,2] Among these systems, J-aggregates of cyanine dyes have been studied abundantly,[3,4] but also bio-organic aggregates, in particular chlorophyll antennae in photosynthetic systems,[5] have received much attention. The key aspects that determine the optical response of these systems are the degree of exciton localization, imposed by energy or interaction disorder, the occurrence of superradiant and dark states, intraband relaxation, and energy transport.

Molecular aggregates may occur in a variety of geometries. Nevertheless, most studies have been performed on linear molecular chains (the standard model for cyanine J-aggregates)[3,4] and molecular rings (in particular, the light-harvesting systems LH2 of purple bacteria).[5−8] An interesting alternative geometry that lately has received growing attention is the tubular one. Much work on such aggregates has been done in the context of chlorosomes of green bacteria.[9−15] Although recently their cylindrical geometry has been disputed,[16] a model of self-assembled tubes with a diameter of the order of 10 nm and a length of 100s of nanometers has been the basis of many investigations of these photosynthetic antenna systems. In addition, tubular aggregates have been prepared synthetically by self-assembly of several types of dye molecules.[17−22] These synthetic cylindrical aggregates are considered of interest as artificial light-harvesting systems, possible energy transport wires, and backbones for organic charge transport systems. As a result of a helical structure, they often show a circular dichroism that strongly depends on frequency and solvent.[23−26]

The synthesis of carbocyanine dyes with amphiphilic substituents[27,28] has led to a particularly interesting new type of self-assembled J-aggregates with a tubular geometry.[17−19] The morphology and absorption spectrum of these aggregates can be influenced strongly by changing the side groups of the monomers or by adding surfactants or alcohols to the solvent.[17,19,29,30] In ref 31 it was shown that a representative of this family of dyes, namely 3,3′-bis(3-sulfopropyl)-5,5′,6,6′-tetrachloro-1,1′-dioctylbenzimidacarbocyanine, also referred to as C8S3, in water forms aggregates with three polarized J-bands. Cryo-TEM experiments revealed that these aggregates possess a double-wall tubular morphology with an outer diameter of 15.6 ± 0.5 nm and a double-wall thickness of 2.4 ± 0.5 nm. In ref 31, this geometrical information was used in the analysis of measured isotropic and polarized absorption spectra in terms of a Frenkel exciton model. This allowed for the construction of a model for the molecular structure of the two concentric cylindrical walls that make up the C8S3 aggregates. Localization of the excitons due to weak diagonal disorder was accounted for.

In the current paper, we extend the previous work by addressing the temperature-dependent dynamical properties of localized excitons in the double-wall C8S3 aggregates. Understanding and controlling these properties is of fundamental

* Address correspondence to this author.
† On leave from S. I. Vavilov State Optical Institute, Birzhevaya Linia 12, 199034 Saint-Petersburg, Russia.

10.1021/jp062983d CCC: $33.50
Published on Web 09/19/2006

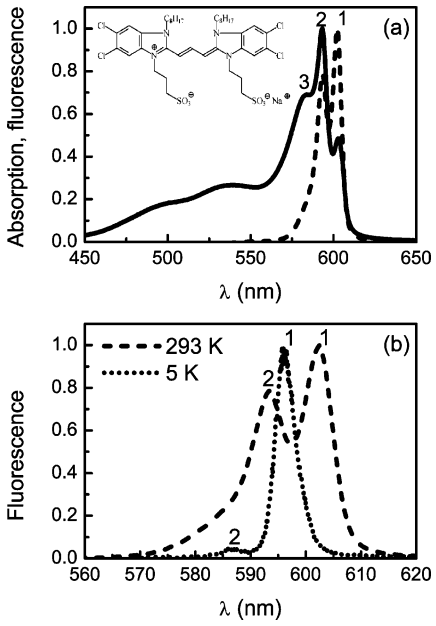

Figure 1. (a) Room temperature absorption (solid line) and fluorescence (dashed line) spectra of C8S3 aggregates. The inset shows the chemical structure of C8S3. (b) Fluorescence spectra of C8S3 aggregates measured at $T = 293$ (dashed line) and 5 K (dotted line). The peak labels are explained in the text.

interest and of crucial importance for prospective light-harvesting and energy-transport applications. Recently, much progress has been made in modeling the exciton dynamics for one-dimensional J-aggregates.[32−34] It is of interest to investigate whether in the case of tubular aggregates similar phenomena are observed and to what extent the models developed can be applied to these systems as well.

To study the exciton dynamics, we have performed time-resolved and steady-state fluorescence experiments, which uncovered ultrafast relaxation between different J-bands as well as within each band. The fluorescence related to the lowest energy J-band is studied in most detail. The time-resolved spectrum reveals a dynamic Stokes shift, while the decay of the fluorescence at each frequency is nonexponential. The steady-state spectrum displays a Stokes shift with a nonmonotonic temperature dependence. We will show that if we add a weak coupling between the localized excitons and a phonon bath, the model constructed previously for the double-wall molecular structure gives good fits to the measurements. To this end, we will treat the dynamics at the level of a Pauli master equation for the exciton populations, with relaxation rates calculated through Fermi's golden rule. This method recently has been proven to give excellent agreement with experiments on a variety of linear cyanine aggregates.[33,34]

The outline of this paper is as follows. In section II we briefly address the sample preparation and the experimental setup. The results of the steady-state and time-resolved fluorescence experiments are presented in section III, where also a first interpretation is offered. In section IV, a more detailed analysis and discussion are given, based on numerical simulations of the Frenkel exciton model with weak exciton−phonon coupling. Finally, we present our conclusions in section V.

II. Sample Preparation and Experimental Setup

Stock solutions of 6.2×10^{-3} M C8S3 (FEW Chemical; see inset of Figure 1 for structure) were prepared by dissolving the dye in doubly distilled water and stirring at room temperature for at least 24 h. At these concentrations, the double-wall tubular aggregates mentioned in the Introduction are formed through self-assembly. A droplet of the solution was squeezed between two 0.12 mm thick microscope cover slips and quenched to 77 K in liquid nitrogen. Subsequently the sample was transported into a He continuous-flow cryostat (CF1204SEG, Oxford Instruments). The sample was irradiated by the frequency-doubled output (495 nm) of a frequency tunable Ti:Sapphire laser (Mira 900, Coherent) generating 120 fs pulses at a repetition rate of 80 MHz. To avoid heating of the sample, a pulse picker was used to reduce the repetition rate to 1.9 MHz. After attenuation to pulse energies of about 0.3 pJ, the beam was focused into the sample with a lens of 10 cm focal length. The resulting excitation density corresponded to the absorption of one photon per 10^6 monomers, thus ensuring absence of exciton−exciton annihilation. Time-resolved fluorescence experiments on the aggregates were performed in the temperature range from 5 to 100 K, using a streak camera system with a synchro-scan sweep unit (Hamamatsu). The time resolution of the experimental setup was 8 ps, as determined by recording the scattered light of the excitation pulse.

III. Experimental Results

A. Steady-State Spectra. The solid line in Figure 1a displays the absorption spectrum of C8S3 aggregates measured at room temperature. Its structure has been explained in ref 31 already: the spectrum is dominated by optical transitions to states in the two weakly coupled exciton bands that are associated with the inner and the outer walls of the tubular aggregates. More specifically, the J-band labeled 1 (2) arises from transitions to lower band-edge exciton states on the inner (outer) wall, polarized parallel to the cylinder axis, while band 3 results from higher exciton transitions polarized perpendicular to this axis. Peak 3 has contributions from both the inner and the outer wall, which cannot be separated due to their large spectral overlap.[31,35,36] Finally, the absorption features in the spectral region 450−550 nm are found to be unpolarized; they are dominated by nonaggregated molecules. Upon decreasing the temperature, the absorption spectrum is shifted to the blue, while keeping the same basic structure with a slight narrowing of the three exciton J-bands. At 5 K the blue-shift amounts to 6−7 nm (not shown).[37]

The dashed curve in Figure 1a displays the room temperature steady-state fluorescence spectrum of the aggregates; the same spectrum is shown in more detail in Figure 1b (dashed), together with the fluorescence spectrum at 5 K (dotted). The room temperature spectrum is dominated by two bands, which fully overlap with the two lowest energy absorption bands 1 and 2. The ratio of the integrated intensities of the measured fluorescence bands is $I_2/I_1 = 0.65 \pm 0.05$. If one assumes that at room temperature phonon-assisted relaxation leads to thermal equilibration of the complete exciton population (in as well as between walls) before emission occurs,[38] one has

$$\frac{I_2}{I_1} = \frac{\int \mathrm{d}E A_2(E) \exp[-E/k_\mathrm{B}T]}{\int \mathrm{d}E A_1(E) \exp[-E/k_\mathrm{B}T]} \qquad (1)$$

where $A_1(E)$ and $A_2(E)$ denote the absorption in the J-bands 1 and 2, respectively, and k_B is the Boltzmann constant. If both bands have approximately the same shape, eq 1 reduces to

$$\frac{I_2}{I_1} = \frac{D_2 \cos^2\theta_2}{D_1 \cos^2\theta_1} \exp[-(E_2 - E_1)/k_B T] \qquad (2)$$

where D_1 (D_2) is the diameter of the inner (outer) tubular wall, θ_1 (θ_2) is the angle between the molecular transition dipoles and the tube axis for the inner (outer) wall, and E_1 and E_2 are the peak frequencies of bands 1 and 2, respectively. Here we invoked the sum rule stating that the integral over the total absorption spectrum of each wall is proportional to the number of molecules in the wall, i.e., proportional to its diameter. Equation 1 yields $I_2/I_1 = 0.4 \pm 0.1$, with the large error deriving from the uncertainty in determining the separate contributions from bands 1 and 2 in the observed absorption spectrum. The simplified expression eq 2 gives $I_2/I_1 = 0.43 \pm 0.05$, where we use $E_2 - E_1 = 280 \pm 5$ cm^{-1}, and the values for D_i and θ_i are taken from ref 31 (also see section IV.A). These results show that at room temperature equilibration between bands 1 and 2 is almost (but not completely) reached on the time scale for emission.

As is observed in Figure 1b, the fluorescence spectrum at 5 K is blue shifted by about 7 nm relative to room temperature, while its peaks are about twice as narrow. Since in the experiments the fluorescence was excited via high-lying states ($\lambda_{ex} = 495$ nm), the two observed fluorescence bands are formed after intraband relaxation from the initially excited states to the optically dominant ones at the band edges. If the inner and outer wall were not coupled, the ratio of excitation in both bands would simply reflect the ratio of the number of molecules in the two cylinders, i.e., their diameters. Hence, the fluorescence intensities would be of the same order. However, the intensity of band 2 is much smaller than that of band 1. This is a clear indication that efficient energy transfer occurs between both cylinders, even at low temperature. At the same time, the fact that band 2 (lying 280 cm^{-1} above band 1) still exhibits any fluorescence at 5 K also demonstrates that the populations of both bands do not reach thermal equilibrium during the exciton lifetime. Apparently, the residual interwall excitation transfer, which takes place after the relaxation to the band edges, occurs at roughly the same time scale as the decay to the ground state. This suggests that transfer of exciton population between both walls mostly takes place during the fast initial relaxation. This transfer may be expedited by the possibility that the higher energy exciton states (well above the optically dominant ones) of both walls are mixed. Thus far, experiments have only shown clear evidence that for the optically dominant states such mixing does not occur;[35,36] in the high-energy region, the degree of mixing is unknown.

B. Spectrally Resolved Fluorescence Decay. More detailed information on the thermalization and decay of the excitons may be obtained from a chronospectroscopic analysis of the fluorescence. Figure 2 shows streak-camera images (upper panels) as well as the spectrally integrated fluorescence decay (lower panels) of bands 1 and 2, recorded at 5 and 100 K, following pulsed excitation at $\lambda_{ex} = 495$ nm. As is seen from the streak-camera data, already at early times the intensity ratio of bands 1 and 2 is strongly in favor of band 1. This supports our conclusion, based on the steady-state spectra, that the energy transfer from the outer to the inner wall predominantly occurs during the fast downward intraband relaxation from the initially excited high-energy states to the optically dominant band-edge ones. The streak-camera images also show that at 5 K the fluorescence peaks exhibit a dynamic Stokes shift, i.e., they shift to higher wavelength during the decay. We will investigate this in more detail in section III.C.

We now turn to the spectrally integrated decay curves in the lower panels of Figure 2. Clearly, this decay is nonexponential and band dependent. In fact, as will be seen from Figure 3 below, even for fluorescence collected within a narrow spectral range the decay remains nonexponential. This originates from the fact that the rates of intra- and interband relaxation as well as the rate of spontaneous emission are distributed over a broad range of values (see section IV).

At 5 K, the integrated fluorescence of the blue band 2 decays with 27 ps as the typical time constant (defined as the time it takes until the intensity decays to 1/e of its peak value). This time constant decreases to 19 ps at 100 K. The observed delayed formation of the fluorescence from the red band 1 (in particular at 5 K) indicates that the decay of band 2 partially results from residual energy transfer from the low-energy exciton states of the outer wall to those of the inner one. The fact that the integrated fluorescence of band 1 decays more slowly (with time constants of 74 and 64 ps at 5 and 100 K, respectively) is consistent with this picture.

Figure 3 shows the fluorescence kinetics for the blue, central, and red parts of band 1 (inner wall) at 5 and 100 K. These curves were obtained by integrating the fluorescence emission over the spectral intervals 590−594, 594−598, and 598−602 nm, respectively. To emphasize the differences in the kinetics for these intervals, the peak intensity for each curve was set to unity. It should be noted that the experimental time resolution does not allow for the detection of the fast intra- and interband relaxation processes from the initially excited states at 495 nm to the optically active band-edge states. Thus, the curves in Figure 3 reflect the kinetics after this initial relaxation has been completed.

At 5 K, the decay time constants for the three spectral intervals clearly differ; they take the values 27, 74, and 97 ps for the blue, the central, and the red part of the band, respectively. These differences arise from the fact that after the fast initial relaxation to the band-edge region, further downward intraband relaxation processes still successfully compete with the radiative emission. Similar behavior has been observed and modeled for one-dimensional exciton systems.[39−41]

Upon increasing the temperature, the fluorescence decay at the blue side of band 1 gradually slows down, while the decay of the red side becomes faster. The reason is that the rates for upward energy transfer between the low-lying states become more and more comparable to the downward rates. From the lower panel of Figure 3, it is evident that at 100 K the fluorescence kinetics are equal for all parts of band 1, indicating that at this temperature the thermalization of the excitons in band 1 is a much faster process than the fluorescence emission. The decay time of 64 ps, common to the three spectral intervals at 100 K, indeed nicely agrees with the time constant obtained upon full integration over band 1 (see above). We finally note that qualitatively similar effects are observed for the fluorescence within band 2. However, due to the low fluorescence intensity and the fast decay in this band, a quantitative characterization of the kinetics is not possible.

C. Dynamic Stokes Shift of the Fluorescence Spectrum. In this section we turn to the dynamic Stokes shift in more detail. Figure 4 presents time-dependent fluorescence spectra at 5 K, obtained by integrating the spectrum over subsequent intervals of 20 ps. On the left-hand side, the development of band 1 (inner wall) is presented, while on the right-hand side, band 2 (outer wall) is followed. It is clearly seen that both bands shift to lower energy as a function of time (dynamic Stokes shift). This confirms the conclusion reached in section III.B that after the

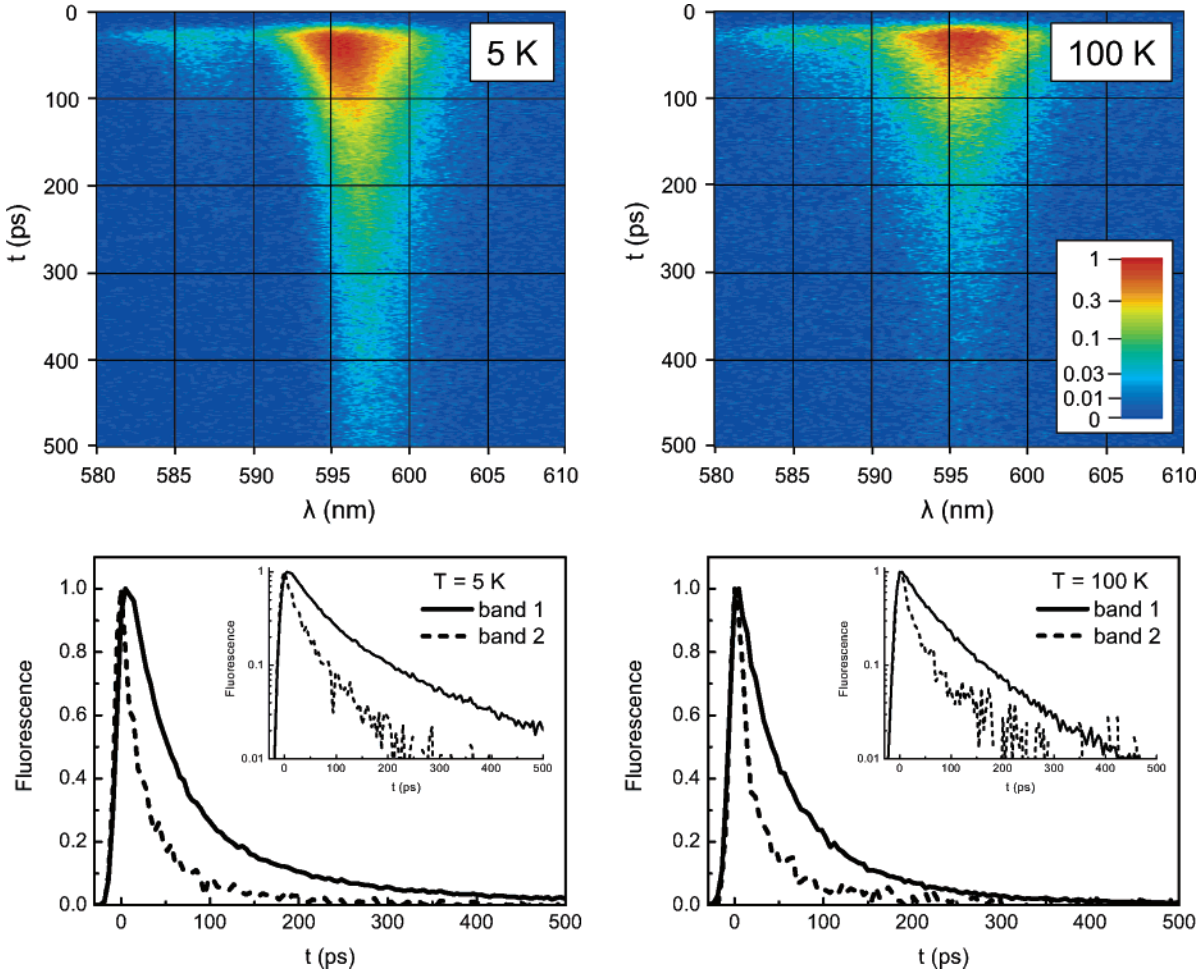

Figure 2. Time-resolved fluorescence dynamics at $T = 5$ (left) and 100 K (right). Upper panels: streak-camera fluorescence signals (logarithmic intensity scale). Lower panels: spectrally integrated fluorescence decay of band 1 (solid line) and band 2 (dashed line). In the inset, the decay is plotted on a logarithmic scale to demonstrate its nonexponential nature.

fast initial relaxation to the band-edge region, the excitons still have a chance to relax to even lower energy states. The spectral dynamics is observed for both fluorescence bands; however, from now on we will focus on band 1, because the dynamics of band 2 is hardly resolved, as noted before. As is seen from Figure 4, the shape of band 1 exhibits a decay of the blue side on a sub-100 ps time scale, followed by a somewhat slower broadening on the red side.

Upon increasing the temperature, the spectral dynamics of band 1 gradually diminishes; above 60 K it is very hard to distinguish any dynamic Stokes shift. This is shown in Figure 5, where we display the streak-camera fluorescence signals for six temperatures, ranging from 5 to 80 K. To enhance the visualization of the spectral dynamics, in each time step the spectra were normalized to have identical maximum intensity. The disappearance of spectral dynamics above 60 K reflects the fact that the thermalization in band 1 then occurs faster than the radiative decay. We already concluded in section III.B that this happens at elevated temperatures, but the data in Figure 5 give a more refined picture of this temperature dependence.

To end this section, we present in Figure 6 the temperature dependence of the center-of-mass position of the steady-state fluorescence associated with band 1, after excitation at $\lambda_{ex} =$ 495 nm. As is observed, the fluorescence first shifts to the red when increasing the temperature from 5 to 15 K and then shifts to the blue when increasing the temperature further. Below 100 K, the absorption spectrum hardly changes at all, so that the shift of the fluorescence band directly reflects changes in the Stokes shift. While for individual molecules the Stokes shift usually decreases monotonically with growing temperature, a nonmonotonic behavior is well-known for exciton systems and has been observed in quantum wells[42,43] and linear J-aggregates.[39] The phenomenon finds its explanation in the fact that at low temperatures the relaxation rates are too small for the exciton system to reach thermal equilibrium within the exciton lifetime.[33,41,42] Specifically, at very low temperatures the excitons do not reach the lowest possible exciton state: the diffusion of excitons is stopped after a few downward-energy jumps because of the low density (and the overlap) of the DOS tail states. When slightly increasing the temperature, the probability to populate yet lower states is favored via diffusion over higher states which overlap with several DOS tail states. More details of the underlying mechanism can be found in refs 32, 33, and 41. It is noteworthy that the temperature at which the maximal red shift occurs and the value of the maximum are practically the same as for the one-dimensional J-aggregates of the dye 3,3′-bis(sulfopropyl)-5,5′-dichloro-9-ethylcarbocyanine (known as THIATS): about 15 K and 5−10 cm^{-1}, respectively.[33,39] It should be noted, however, that the experimental error bars are large, which makes it hard to unambiguously decide on the range of the nonmonotonic behavior. We will return to this in section IV.B.

IV. Model Calculations

A. Aggregate Structure and Absorption Spectrum. With use of data from cryo-TEM as well as the isotropic absorption

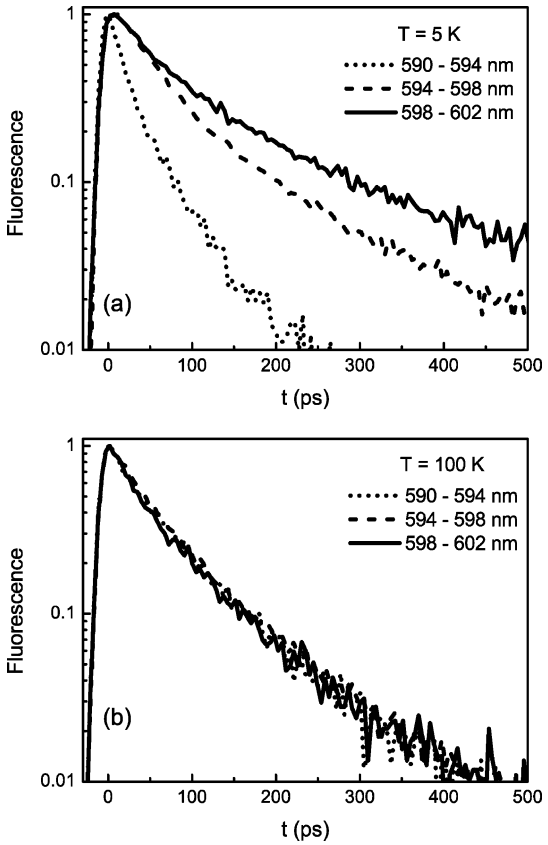

Figure 3. Fluorescence decay of band 1 in different spectral intervals measured at 5 (a) and 100 K (b). All curves were normalized to the same peak intensity.

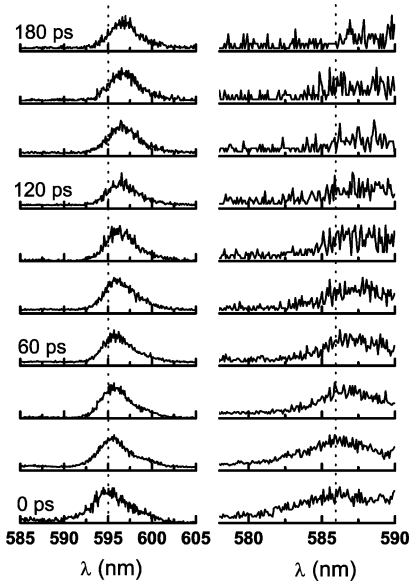

Figure 4. Fluorescence spectra integrated over subsequent time intervals of 20 ps for the inner wall (left) and the outer wall (right) of tubular C8S3 aggregates. All spectra were normalized to have the same peak intensity.

and linear dichroism spectra, a structural and electronic model for the double-wall J-aggregates of C8S8 has previously been proposed.[31] Here we briefly describe this model and present numerical results for the absorption spectrum, the density of states, and the oscillator strength per state. In section IV.B, we will extend the model to account for exciton−phonon scattering and compare the resulting temperature-dependent spectral dynamics to experiment.

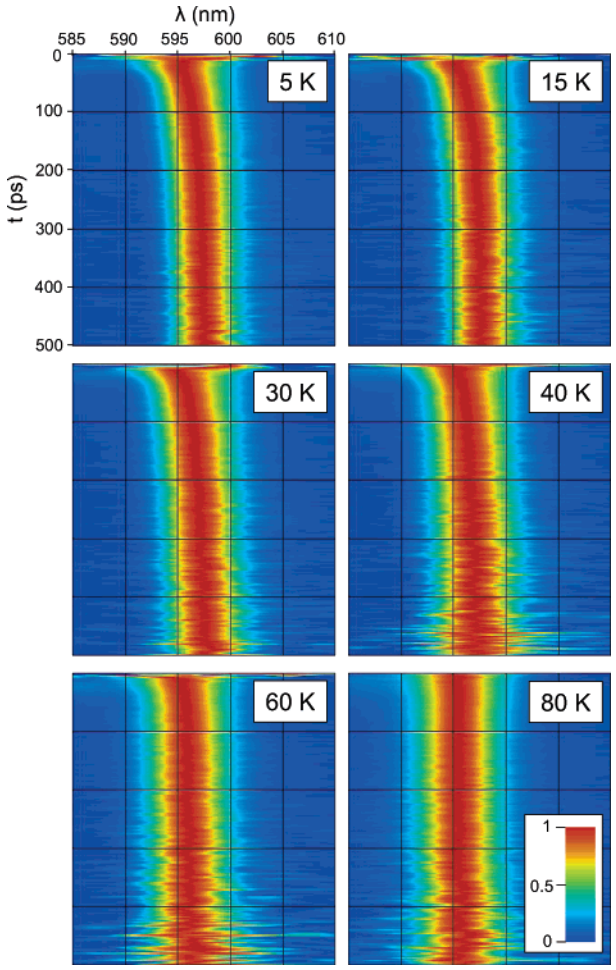

Figure 5. Spectral dynamics in band 1 (inner wall) of C8S3 aggregates. At each time step the fluorescence spectrum was normalized to the same peak intensity. The observed broadening of the spectra at higher temperatures and at long delay times is an artifact caused by weak fluorescence.

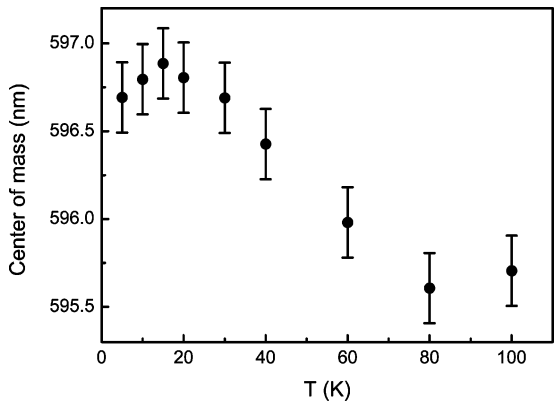

Figure 6. Temperature dependence of the center-of-mass position of the fluorescence band 1.

The structural model proposed for the double-wall aggregates in ref 31 consists of two concentric cylinders of diameters $D_1 = 10.9$ nm and $D_2 = 15.6$ nm. To define the molecular positions on these cylinders, each of them is constructed by wrapping a two-dimensional brick-layer lattice on a cylinder of the proper diameter. Each brick represents a C8S3 molecule and has a length $a = 2$ nm and a width $d = 0.4$ nm, to conform with the known size of the molecule.[44] Adjacent bricks are shifted relative to each other along their long axis over a distance s. The direction in which the lattice is rolled on the cylinder distin-

guishes different tubular aggregates. This direction is uniquely defined by the angle θ that the long axis of each brick (i.e., the transition dipole of each C8S3 molecule) makes with the cylinder axis. The parameters s and θ are not known a priori; in ref 31 they have been used as free parameters to fit the positions and the intensities of the exciton peaks in the room temperature absorption and linear dichroism spectra. This gave $s = 0.24a$ and $\theta = 43.0°$ for the outer cylinder and $s = 0.25a$ and $\theta = 47.4°$ for the inner one.

The electronic excitations of the tubular aggregates are modeled by a Frenkel exciton Hamiltonian in which each molecule (located at one of the brick positions) is considered a two-level system and dipole−dipole transfer interactions give rise to delocalized excited states. In the model, the exciton bands of both walls are considered as decoupled. In the optically dominant band-edge region this simplification is justified because pump−probe spectroscopy reveals that the excitons in the absorption bands 1 and 2 do not have a common ground state.[35,36] Of course, interwall electronic interactions exist, but in the band-edge region, instead of mixing of the exciton states of both walls, they give rise to incoherent energy transfer from the outer wall to the inner one. In section III.A, we found indications for such transfer; more detailed insight, revealing a transfer time of 275 ps at room temperature, has been obtained in ref 36.

Thus, each of the walls is described by a Hamitonian[45,46]

$$H_0 = \sum_n \omega_n |n\rangle\langle n| + \sum_{n,m}{}' J_{nm} |n\rangle\langle m| \qquad (3)$$

where $|n\rangle$ denotes the state in which the molecule n is excited and all the other molecules are in their ground state. Furthermore, ω_n denotes the transition energy of molecule n (we set $\hbar = 1$) and J_{nm} is the excitation transfer interaction between molecules n and m (the prime on the summation excludes the term with $m = n$). We model static disorder by treating the ω_n as stochastic variables, while for the J_{nm} we use the extended dipole model

$$J_{nm} = C\frac{\mu^2}{l^2}\left[\frac{1}{r_{nm}^{++}} - \frac{1}{r_{nm}^{+-}} - \frac{1}{r_{nm}^{-+}} + \frac{1}{r_{nm}^{--}}\right] \qquad (4)$$

Here, $C = 5.04\ \mathrm{cm^{-1}\ nm^3/D^2}$, $\mu = Ql$ is the molecular transition dipole moment formed by two point charges Q and $-Q$ separated by a distance l, and r_{nm}^{++}, r_{nm}^{+-}, r_{nm}^{-+}, and r_{nm}^{--} are the distances between the effective charges of molecules n and m.[31] From semiempirical calculations it is found that $l = 0.7$ nm and $Q = 0.34e$,[47] with e the electron charge; this gives $\mu = 11.4$ D.

The absorption spectrum of the double-wall tubular aggregates is now obtained by adding the spectra of the two decoupled exciton systems. Denoting by E_ν and $\varphi_{\nu n}$ the eigenvalues and eigenvectors, respectively, of the Hamiltonian eq 3, the spectrum of one cylinder reads

$$A(E) = \left\langle \sum_\nu F_\nu \delta(E - E_\nu) \right\rangle \qquad (5)$$

where $F_\nu = (\sum_n \varphi_{\nu n})^2$ is the dimensionless oscillator strength of the νth exciton state and the angular brackets denote the average over the disorder realizations. By taking the ω_n uncorrelated from a Gaussian distribution with mean $\omega_0 = 19\,194\ \mathrm{cm^{-1}}$ ($\lambda = 521$ nm) and a standard deviation $\sigma = 670\ \mathrm{cm^{-1}}$, and by using the other model parameters given above, good fits are obtained to the room temperature absorption and linear dichroism spectra of the double-wall aggregates.[31]

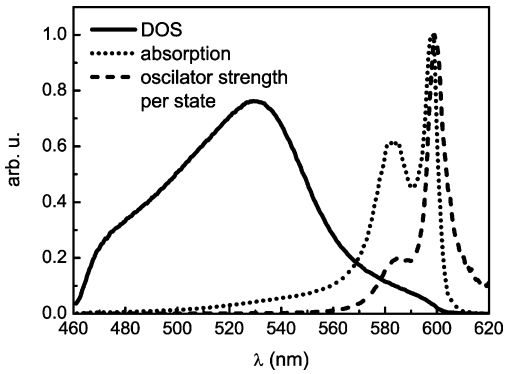

Figure 7. Density of states (solid line), absorption spectrum (dotted line), and oscillator strength per state (dashed line), calculated for the inner cylinder within the model described in section IV.A.

In ref 31 the spectra were calculated by using the coherent potential approximation (CPA), instead of the nowadays more customary brute-force numerical simulations. The reason for using the CPA is the sheer size of the aggregates. The inner (outer) wall contains 43 (62) molecules per nanometer length. Thus, to model a tube of a length that is larger than its circumference, one has to handle systems of at least a few thousand coupled molecules. Brute-force simulations for such systems (with long-range interactions) are demanding. Fortunately, it is well-known that to calculate absorption spectra, the CPA provides an excellent method.

In the current paper, however, we will be interested in modeling the exciton dynamics, which is considerably more involved than the absorption spectrum and cannot be done with the CPA. Therefore, we resort to numerical simulations afterall. To keep the problem at least reasonably tractable, we will focus entirely on the spectral dynamics in the frequency region of band 1. As this is the lowest excitonic band, which results from the inner cylinder and lies about 280 $\mathrm{cm^{-1}}$ below band 2 of the outer cylinder, one expects that up to about 100 K ($k_BT \approx 70\ \mathrm{cm^{-1}}$) the spectral dynamics in band 1 may be well described by considering just the inner cylinder. Upward energy transfer to band 2 may safely be neglected under these conditions.

Figure 7 gives our results for the density of states $\rho(E) = \langle \sum_\nu \delta(E - E_\nu) \rangle$ (solid line), the absorption spectrum $A(E)$ (dotted line), and the average oscillator strength per state $F(E) = A(E)/\rho(E)$ (dashed line), obtained by numerically simulating the above model for the inner cylinder. The data shown were obtained for a system of 4000 molecules, which corresponds to a cylinder length of about 93 nm. All results have converged as a function of this length. The DOS reveals tails that extend outside the exciton band that exists for the system without disorder (not shown). These tails result from disorder-induced localization. The states which dominate the absorption and fluorescence spectra are located in the low-energy tail. Two absorption peaks can be distinguished. The one at 600 nm is polarized along the tube axis and is responsible for the measured absorption band 1. The peak at about 582 nm is polarized perpendicular to the axis and contributes to the measured band 3. We note that the simulated absorption spectrum agrees with the spectrum for the inner tube obtained in ref 31 using the CPA.

It appears from Figure 7 that the average oscillator strength per state varies quite strongly over the absorption bands. In fact, a more detailed analysis reveals that, at each given frequency, the oscillator strength per state shows strong fluctuations, as a consequence of the disorder (cf. ref 41). This gives rise to strong

variations in the spontaneous emission rates, which explains qualitatively the nonexponential character of the decay of the integrated fluorescence intensity reported in section III.B. The observed frequency-dependent fluorescence kinetics, as well as the (dynamic) Stokes shift of the fluorescence spectra, originate from the relaxation of excitons within the tail of the DOS. The model for this relaxation will be presented in the next section.

B. Modeling the Spectral Dynamics. We model the exciton dynamics in the inner wall, with a special interest in the spectral dynamics in band 1, by using the Pauli master equation for the populations P_ν of the exciton states:

$$\dot{P}_\nu = R_\nu - \gamma_\nu P_\nu + \sum_{\mu=1}^{N} (W_{\nu\mu} P_\mu - W_{\mu\nu} P_\nu) \tag{6}$$

Here, R_ν is a source term that models the excitation of the system (to be specified lateron) and $\gamma_\nu = \gamma_0 F_\nu$ is the spontaneous emission rate of the νth exciton state, where γ_0 is the spontaneous emission rate of a monomer. Due to the strong tendency of the dye molecules to form aggregates in water, it is close to impossible to determine γ_0 in this solvent. We will therefore treat it as a fit parameter. Finally, $W_{\mu\nu}$ is the scattering rate from the localized exciton state $|\nu\rangle$ to the state $|\mu\rangle$, resulting from weak exciton−vibration coupling.

By restricting ourselves to one-phonon-assisted exciton scattering, we obtain[34,40,48]

$$W_{\mu\nu} = \mathcal{F}(|\omega_{\mu\nu}|)\, I_{\mu\nu} \times \begin{cases} n(\omega_{\mu\nu}), & \omega_{\mu\nu} > 0 \\ n(-\omega_{\mu\nu}) + 1, & \omega_{\mu\nu} < 0 \end{cases}$$

where $\omega_{\mu\nu} = E_\mu - E_\nu$ and $\mathcal{F}(\omega) = 2\pi \sum_q |V_q|^2 \delta(\omega - \omega_q)$ is the one-phonon spectral density of the bath (ω_q is the energy of a phonon in mode q and V_q characterizes the coupling of this mode to the excitons). Furthermore, $I_{\mu\nu} = \sum_n \varphi_{\mu n}^2 \varphi_{\nu n}^2$ is the overlap integral of the exciton site probabilities in the states μ and ν, and $n(\omega) = [\exp(\omega/k_B T) - 1]^{-1}$ is the mean occupation number of a phonon with energy ω. By construction, these transition rates meet the principle of detailed balance: $W_{\nu\mu} = W_{\mu\nu} \exp(\omega_{\mu\nu}/k_B T)$. Thus, if the intraband relaxation dominates over the radiative decay, the excitons will thermalize to the Boltzmann distribution prior to emission.

Lacking detailed knowledge of the density of states of the vibrations in the solvent as well as the energy dependence of their coupling to the excitons, we will resort to using a model function of the one-phonon spectral density,

$$\mathcal{F}(\omega) = W_0 \frac{\omega}{\omega_c} \left(1 + \eta \frac{\omega}{\omega_c}\right) \exp\left(-\frac{\omega}{\omega_c}\right) \tag{7}$$

This reflects Ohmic (linear) behavior for small energies,[49] with quadratic corrections at higher energies and a cutoff beyond ω_c. The parameter W_0 (characterizing the overall scattering strength) is treated as a free parameter and used to fit the experiments, while we have fixed $\eta = 1$ and $\omega_c = 100$ cm^{-1}.[50] A spectral function of this form has been applied successfully to fit the optical dynamics in photosynthetic antenna complexes[50−53] and to model ultrafast electron-transfer processes.[54−56] Other power laws have been considered as well. Specifically, an ω^3 scaling of $\mathcal{F}(\omega)$, characteristic for scattering on long-wavelength acoustic phonons, has been shown to yield excellent fits of the observed temperature-dependent spectral dynamics of linear J-aggregates of pseudoisocyanine.[34]

By making use of the Pauli master equation, we have simulated the dynamics of the exciton populations on the inner wall, taking as input the exciton energies and eigenfunctions obtained from the simulations described in section IV.A. In accordance with the excitation conditions in the fluorescence experiments, we set $R_\nu(t) = F_\nu S(t)$ for E_ν in a narrow window centered at $\lambda_{ex} = 495$ nm; outside this window we took $R_\nu = 0$. Here, $S(t) = S =$ constant for steady-state response, while $S(t) = S\delta(t)$ to simulate the pulsed experiments.

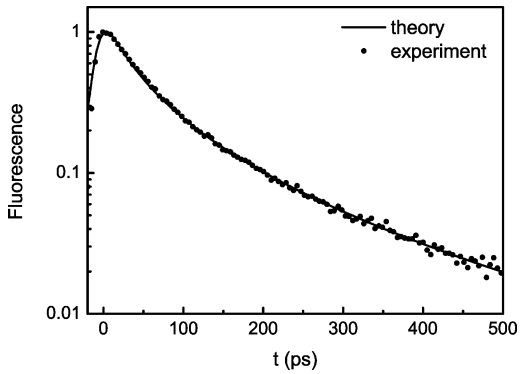

Figure 8. Comparison between the simulated (solid line) and measured (dots) integrated fluorescence decay of band 1 at $T = 5$ K (cf. solid line in Figure 2a).

From the solution of the Pauli master eq 6, the time-dependent fluorescence intensity at energy E is calculated according to the definition

$$I(E,t) = \left\langle \sum_\nu \gamma_\nu P_\nu(t) \delta(E - E_\nu) \right\rangle \tag{8}$$

For steady-state response, the $P_\nu(t)$ are simply replaced by the steady-state solutions. The results presented in Figures 8−10 were obtained by using a scattering strength of $W_0 = 5200$ cm^{-1} and a monomer emission rate of $\gamma_0 = 2.95 \times 10^8$ s^{-1}, which generated good fits of the measurements. The average was calculated over 1000 disorder realizations. We stress that W_0 and γ_0 are the only fit parameters in the current work; all other model parameters have been taken from analyzing the linear spectra and the cryo-TEM experiments.[31] The value for γ_0 is of the same order of magnitude as its measured value in methanol (8×10^8 s^{-1}) and similar to the emission rate of the related dye molecule pseudoisocyanine in water (2.7×10^8 s^{-1}). The value of W_0, seemingly high, should not be taken as a typical transfer rate; the latter is strongly reduced compared to W_0 due to the probability overlap $I_{\mu\nu}$, which is of the order of the inverse localization size of the excitons.[33] It turns out that for our model parameters, the typical rates between spatially overlapping optically active states is of the same order of magnitude as their energy difference (∼100 cm^{-1}). This implies that we are just at the limit of the applicability of our approach, which assumes that a perturbative treatment of the exciton−phonon coupling is valid.

Figure 8 shows the decay of the calculated fluorescence intensity integrated over the lowest absorption band for $T = 5$ K (solid line), compared against the experimental data for 5 K (dots). In the calculated curve, we accounted for the finite response time of the streak camera (∼8 ps) by convoluting with its response function. We see that the model reproduces the nonexponential decay in an excellent way. As discussed above, the wide distribution of the oscillator strength per state is the underlying reason for the nonexponentiality. Figure 9 (upper panels) shows the time evolution of the fluorescence spectrum, calculated for $T = 5$ and 80 K. For comparison, the experimental data for these temperatures are plotted directly below. Clearly, the simulated spectra follow the same tendency as the measured ones, with a marked dynamic Stokes shift at low temperatures,

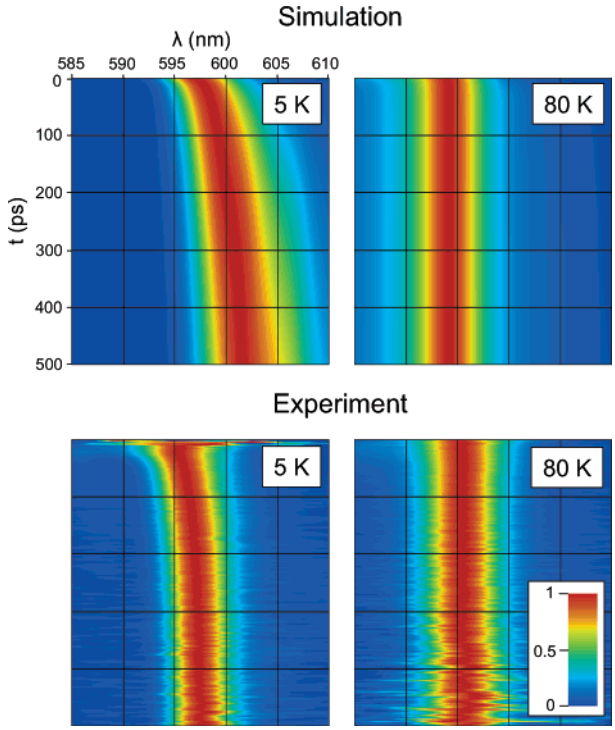

Figure 9. Simulated (upper panels) and measured (lower panels) time-dependent fluorescence spectra at low temperature and elevated temperature. The spectra are normalized to the same peak intensity at each time step.

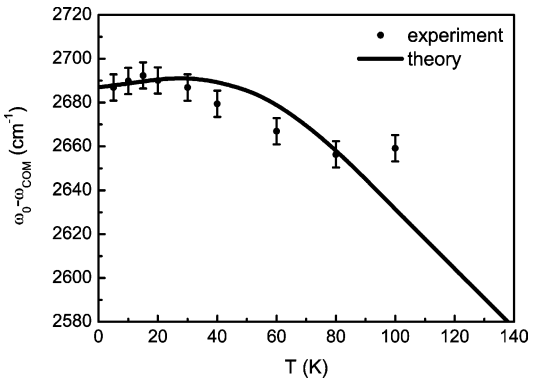

Figure 10. Temperature dependence of the center-of-mass frequency of the lowest energy *J*-band in the simulated steady-state fluorescence spectrum (solid line), compared to experiment (dots).

which vanishes when increasing T. The explanation is that at low temperatures the excitons continue to relax downward in the tail of the DOS during the emission process, while upon heating the exciton population equilibrates over the J-band 1 on the time scale of emission.

To demonstrate quantitatively the similarity of the simulated and the measured spectra, we have also calculated the temperature dependence of the center-of-mass position ω_{COM} of the steady-state fluorescence band 1. As stated in section III.C, below 100 K the changes in this position directly reflect changes in the Stokes shift. In Figure 10 the results are compared to the measurements of Figure 6, by plotting $\omega_0 - \omega_{COM}$, with ω_0 the monomer transition frequency. We see that the theory reproduces the nonmonotonic temperature dependence originating from a lack of equilibration at low temperatures (see section III.C) and until about 80 K follows the trend of the experimental data rather well. The nonmonotonic range, however, seems rather weak—almost plateau-like—as compared to the experiment. For the one-dimensional aggregates of the dye THIATS, simulations revealed a much stronger nonmonotonic range.[33,41] This may be due to the fact that the long-range interactions in the locally two-dimensional cylinders give rise to different localization properties of eigenstates than in one dimension. In particular, long tails may exist in these states, as has been shown by a study of the autocorrelation function of the wave function in ref 57. We note that beyond 80 K, the agreement between theory and experiment fails, even qualitatively, possibly as a result of the fact that our Master equation approach does not account for the vibration-induced loss of coherence within exciton localization domains.[34]

V. Summary and Concluding Remarks

We have performed steady-state and time-resolved fluorescence experiments to unravel the temperature-dependent spectral dynamics of Frenkel excitons in the double-wall cylindrical J-aggregates of the dye C8S3. The experiments have been analyzed by making use of the aggregate structure and model Hamiltonian that had been proposed in ref 31 to fit the absorption and linear dichroism spectra. To describe the exciton dynamics, we extended the model to account for weak exciton—phonon scattering. Two new free parameters were introduced: the overall scattering strength W_0 and the monomer spontaneous emission rate γ_0. The model yields good fits to the experiments.

Each cylindrical wall gives rise to one narrow fluorescence J-band. The lowest energy one of these (band 1) results from radiative decay of excitons from the inner wall; band 2, which is about 280 cm^{-1} higher in energy, is due to excitons on the outer wall. At room temperature, the steady-state fluorescence of these bands has an intensity ratio close to unity. As we have shown, at this temperature equilibration between the excitons in band 1 and band 2 is almost, but not completely, reached on the time scale of spontaneous emission. At low temperatures, band 2 undergoes strong quenching due to fast energy transfer to band 1. Still band 2 is visible, even at temperatures as low as 5 K, which demonstrates that at these temperatures, on the time scale of emission, the system stays far from thermal equilibrium between both bands.

The time-resolved experiments revealed that the fluorescence decay is nonexponential. This results from the fact that disorder generates a wide spread in the oscillator strength per state. Band 2 always decays faster than band 1, while within band 1 the blue part of the fluorescence decays faster than the red part. These differences find their origin in inter- and intraband relaxation. Above 60 K, the differences in decay times within band 1 disappear, reflecting thermalization of the excitons within this band on a time scale faster than the emission time. In agreement with this, we also found a dynamic Stokes shift of band 1, which gradually diminishes when increasing T and has completely vanished above about 60 K.

The crossover from a nonequilibrium to a thermalized distribution of exciton populations within band 1 on the time scale of spontaneous emission is also reflected in a nonmonotonic temperature dependence of its steady-state Stokes shift. At low temperatures, the Stokes shift grows with temperature and reaches a maximum at about 15 K, before it decreases again. Such a nonmonotonic behavior arises from the fact that at low temperature, blockage of the downward-energy diffusion prevents the excitons to reach thermal equilibrium before emission.

A further study of the exciton dynamics in these aggregates should focus on the energy transfer from the outer wall to the inner wall as well as the transport within the walls. Indications for fast interwall transfer have been reported in this paper already; a more detailed quantitative analysis, based on pump—probe spectroscopy, is in progress.

Acknowledgment. This work is part of the research program of the Stichting voor Fundamenteel Onderzoek der Materie (FOM), which is financially supported by the Nederlandse Organisatie voor Wetenschappelijk Onderzoek (NWO). Support was also received from NanoNed, a national nanotechnology program coordinated by the Dutch Ministry of Economic Affairs.

References and Notes

(1) Jelley, E. E. *Nature* **1936**, *138*, 1009.
(2) Scheibe, G. *Angew. Chem.* **1936**, *49*, 563.
(3) *J-Aggregates*; Kobayashi, T., Ed.; World Scientific: Singapore, 1996.
(4) Knoester, J. In *Organic Nanostructures*: *Science and Application*; Agranovich, V. M., La Rocca G. C., Eds.; IOS Press: Amsterdam, The Netherlands, 2002; p 149.
(5) Van Amerongen, H.; Valkunas, L.; van Grondelle, R. *Photosynthetic Excitons*; World Scientific: Singapore, 2000.
(6) McDermott, G.; Prince, S. M.; Freer, A. A.; HawthornthwaiteLawless, A. M.; Papiz, M. Z.; Cogdell, R. J.; Isaacs, N. W. *Nature* **1995**, *374*, 517.
(7) Koepke, J.; Hu, X.; Muenke, C.; Schulten, K.; Michel, H. *Structure* **1996**, *4*, 581.
(8) Van Oijen, A. M.; Ketelaars, M.; Köhler, J.; Aartsma, T. J.; Schmidt, J. *Science* **1999**, *285*, 400.
(9) Staehelin, L. A.; Golecki, J. R.; Drews, G. *Biochim. Biophys. Acta* **1980**, *589*, 30.
(10) Betti, J. A.; Blankenship, R. E.; Natarajan, L. V.; Dickenson, L. C.; Fuller, R. C. *Biochim. Biophys. Acta* **1982**, *680*, 194.
(11) Holzwarth, A. R.; Schaffner, K. *Photosynth. Res.* **1994**, *41*, 225.
(12) Prokhorenko, V. I.; Steensgaard, D. B.; Holzwarth, A. R. *Biophys. J.* **2000**, *79*, 2105.
(13) Van Rossum, B. J.; Boender, G. J.; Mulder, F. M.; Raap, J.; Balaban, T. S.; Holzwarth, A. R.; Schaffner, K.; Prytulla, S.; Oschkinat, H.; De Groot H. J. M. *Spectrochim. Acta, Part A* **1998**, *54*, 1167.
(14) Prokhorenko, V. I.; Steensgaard, D. B.; Holzwarth, A. R. *Biophys. J.* **2003**, *85*, 3173.
(15) Didraga, C.; Klugkist, J.; Knoester, J. *J. Phys. Chem.* **2002**, *106*, 11474.
(16) Pšenčík, J.; Ikonen, T. P.; Laurinmäki, P.; Merckel, M. C.; Butcher, S. J.; Serimaa, R. E.; Tuma, R. *Biophys. J.* **2004**, *87*, 1165.
(17) von Berlepsch, H.; Böttcher, C.; Ouart, A.; Burger, C.; Dähne, S.; Kirstein, S. *J. Phys. Chem. B* **2000**, *104*, 5255.
(18) von Berlepsch, H.; Ouart, A.; Regenbrecht, M.; Akari, S.; Keiderling, U.; Schnablegger, H.; Dähne, S.; Kirstein, S. *Langmuir* **2000**, *16*, 5908.
(19) von Berlepsch, H.; Kirstein, S.; Hania, R.; Didraga, C.; Pugžlys, A.; Böttcher, C. *J. Phys. Chem. B* **2003**, *107*, 14176.
(20) Hill, J. P.; Jin, W.; Kosaka, A.; Fukushima, T.; Ichihara, H.; Shinomura, T.; Ito, K.; Hashizume, T.; Ishii, N.; Aida, T. *Science* **2004**, *304*, 1481.
(21) Gandini, S. C. M.; Gelamo, E. L.; Itri, R.; Tabak, M. *Biophys. J.* **2003**, *85*, 1259.
(22) Rotomskis, R.; Augulis, R.; Snitka, V.; Valiokas, R.; Liedberg, B. *J. Phys. Chem. B* **2004**, *108*, 2833.
(23) DeRossi, U.; Dähne, S.; Meskers, C. J.; Dekkers, P. J. M. *Angew. Chem.* **1996**, *108*, 827.
(24) Spitz, C.; Dähne, S.; Ouart, A.; Abraham, H.-W. *J. Phys. Chem. B* **2000**, *104*, 8664.
(25) Kirstein, S.; von Berlepsch, H.; Böttcher, C.; Burger, C.; Ouart, A.; Reck, G.; Dähne, S. *ChemPhysChem* **2000**, *1*, 146.
(26) Didraga, C.; Knoester, J. *J. Chem. Phys.* **2004**, *121*, 946.
(27) Pawlik, A.; Kirstein, S.; DeRossi, U.; Dähne, S. *J. Phys. Chem. B* **1997**, *101*, 5646.
(28) Pawlik, A.; Ouart, A.; Kirstein, S.; Abraham, H.-W.; Dähne, S. *Eur. J. Org. Chem.* **2003**, 3065.
(29) Spitz, C.; Knoester, J.; Ouart, A.; Dähne, S. *Chem. Phys.* **2002**, *275*, 271.
(30) von Berlepsch, H.; Kirstein, S.; Böttcher, C. *Langmuir* **2002**, *18*, 7699.
(31) Didraga, C.; Pugžlys, A.; Hania, P. R.; von Berlepsch, H.; Duppen, K.; Knoester, J. *J. Phys. Chem. B* **2004**, *108*, 14976.
(32) Malyshev A. V.; Malyshev, V. A.; Domínguez-Adame, F. *Chem. Phys. Lett.* **2003**, *371*, 417. Malyshev A. V.; Malyshev, V. A.; Domínguez-Adame, F. *J. Phys. Chem. B* **2003**, *107*, 4418.
(33) Bednarz, M.; Malyshev, V. A.; Knoester, J. *Phys. Rev. Lett.* **2003**, *91*, 217401.
(34) Heijs, D. J.; Malyshev, V. A.; Knoester, J. *Phys. Rev. Lett.* **2005**, *95*, 177402.
(35) Pugžlys, A.; Hania, P. R.; Didraga, C.; Knoester, J.; Duppen, K. *Solid State Phenom.* **2004**, *97*−*98*, 201.
(36) Pugžlys, A.; Hania, P. R.; Didraga, C.; Malyshev, V.A.; Knoester, J.; Duppen, K. In *Ultrafast Phenomena XIV*; Kobayashi, T., Okada, T., Nelson, K. A., De Silvestri, S., Eds.; Springer: New York, 2005; p 879.
(37) At low temperatures, light scattering in the sample makes it impossible to measure the absorption line shape with sufficient accuracy; only the position of the peaks can then be measured reasonably well.
(38) Room temperature pump−probe experiments reveal that a fast ($\tau \approx 275$ fs) inter-wall energy transfer occurs in these systems (see ref 36).
(39) Scheblykin, I. G.; Sliusarenko, O. Yu.; Lepnev, L. S.; Vitukhnovsky A. G.; Van der Auweraer, M. *J. Phys. Chem. B* **2001**, *105*, 4636.
(40) Shimizu, M.; Suto, S.; Goto, T. *J. Chem. Phys.* **2001**, *114*, 2775.
(41) Bednarz, M.; Malyshev, V. A.; Knoester, J. *J. Chem. Phys.* **2004**, *120*, 3827.
(42) Zimmermann, R.; Runge, E. *Phys. Status Solidi A* **1997**, *164*, 511.
(43) Grassi Alessi, M.; Fragano, F.; Patanè, A.; Capizzi, M.; Runge, E.; Zimmermann, R. *Phys. Rev. B* **2000**, *61*, 10985.
(44) Czikkely, V.; Försterling, H. D.; Kuhn, H. *Chem. Phys. Lett.* **1970**, *6*, 11.
(45) Agranovich, V. M. *Zh. Exp. Teor. Fiz.* **1959**, *37*, 430 [English translation: *Sov. Phys. JETP* **1960**, *37*, 307]. Agranovich, V. M. *Fiz. Tverd. Tela* **1961**, *3*, 811 [English translation: *Sov. Phys Solid State* **1961**, *3*, 592].
(46) Davydov, A. S. *Theory of Molecular Excitons;* Plenum: New York, 1971.
(47) Kirstein, S. Private communication.
(48) Bednarz, M.; Malyshev, V. A.; Knoester, J. *J. Chem. Phys.* **2002**, *117*, 6200.
(49) Weiss, Q. *Quantum Dissipative Systems*; World Scientific: Singapore, 1993.
(50) Renger, T.; May, V.; Kühn, O. *Phys. Rep.* **2001**, *343*, 137.
(51) Kühn, O.; Sundström, V. *J. Chem. Phys. B* **1997**, *107*, 4154.
(52) May, V.; Kühn, O. *Charge and Energy Transfer Dynamics in Molecular Systems*; Wiley-VCH: Berlin, Germany, 2000.
(53) Brüggemann, B.; Szenee, K.; Novoderzhkin, V.; van Grondelle, R.; May, V. *J. Phys. Chem. B* **2004**, *108*, 13536.
(54) Egorova, D.; Kühl, A.; Domcke, W. *Chem. Phys.* **2001**, *268*, 105.
(55) Kleinkathöfer, U.; Kondov, I.; Schreiber, M. *Chem. Phys.* **2001**, *268*, 121.
(56) Egorova, D.; Thoss M.; Domcke, W. *J. Chem. Phys.* **2003**, *119*, 2761.
(57) Didraga, C.; Knoester, J. *J. Chem. Phys.* **2004**, *121*, 10687.